Electronic Supplementary Information for

Unit Cell Distortion and Surface Morphology Diversification in SnTe/CdTe(001) Topological Crystalline Insulator Heterostructure: Influence of Defects' Azimuthal Distribution

A. Sulich[1]*, E. Łusakowska[1], W. Wołkanowicz[1], P. Dziawa[1], J. Sadowski[1,3], B. Taliashvili[1], T. Wojtowicz[2], T. Story[1, 2], and J. Z. Domagala[1]

[1]Institute of Physics, Polish Academy of Sciences, Aleja Lotnikow 32/46, PL-02-668 Warsaw, Poland

[2]International Research Centre MagTop, Institute of Physics, Polish Academy of Sciences, Aleja Lotnikow 32/46, PL-02-668 Warsaw, Poland

[3]Department of Physics and Electrical Engineering, Linnaeus University, 391 82 Kalmar, Sweden.

sulich@ifpan.edu.pl

Contents

1. The list of investigated samples

The list of investigated samples is shown in Table S1 together with the values of SnTe layer thickness and the growth conditions (Te/SnTe molecular flux ratio).

Table S1. The list of investigated samples.

Sample number[1)]	**SnTe layer thickness** [nm]	**Te/SnTe molecular flux ratio[2, 3)]**
S1	20	0.0093
S2	80	0
S3	80	0
S4	80	0.0091
S5	500	0
S6	500	0.0093
S7	888	0.0156
S8	1000	0
S9*	1000	0
S10	1000	0.0051
S11*	1000	0.0089
S12	1000	0.0093
S13	1000	0.0135

[1)]* The temperature of substrate during the growth process was typical 310°C; only in the case of S9 and S11 sample it was different: 370°C and 270°C, respectively.

[2)] SnTe flux j_{SnTe} = (4.75±0.85) × 10^{-7} mbar. The average value was 4.5 × 10^{-7} mbar.

[3)] The Te/SnTe molecular flux ratio is a ratio of the fluxes (measured as a pressure) of Te and SnTe obtained from three effusion cells: two with SnTe (binary source) and one with Te.

2. Selection of Bragg reflections for X-ray diffraction measurements

The measurements were done for both symmetrical and asymmetrical of 004 (for GaAs, CdTe and SnTe), -1-15 (for CdTe) and -2-26 (for SnTe) Bragg reflections. Such a choice is dictated by the necessity to measure the possible deformation of the crystal lattice of the tested layers. The name of "symmetrical" reflections is related to the fact that for planes reflecting X rays, the angle of incidence relative to the sample surface is almost equal to the angle of reflection. Such crystallographic planes (in our case (001)) are almost parallel to the sample surface. Name – "asymmetric" reflections is associated with reflections from strongly inclined planes (several to several dozen degrees) to the sample surface. From the symmetric reflection we get the vertical parameter of the unit cell (or call in this paper "out of plane", $a_{\perp}$). With its help, we calculate the size of the unit cell in the interface plane (we use term "in plane", $a_{\parallel}$) from the asymmetric reflections. The area probed was about 2.5±0.5 mm^2. The reflection 224 proposed by Schreyeck et al. in the paper [1] could not be used with our sample growth orientation (001), because of the high asymmetry of the reflex (the angle of mutual inclination of the planes (112) and (001) for CdTe is 35.3°, θ_{224} = 35.6° so $\omega = \theta_{224}$-35.03° = 0.27°) and 2° off-cut affected the ω.

3. Assessment of a general crystallographic quality of samples

The assessment of a general degree of sample crystallographic quality is based on full width at half maximum (FWHM) value of ω-scan curves recorded via open detector (Rocking Curves, *RCs (DA)*). This parameter is under the influence of the total number of defects in the crystal lattice and also provides information concerning substrate off-cut magnitude and direction as well as crystallographic plane misorientation (tilt) of a layer (the scheme of off-cut and tilt is shown in Figure 1 in the article).

3.1. Defects concentration

Generally, the value RC (DA) FWHM is high when there are many defects in a crystal. Besides, it enfolds also a contribution from experimental setup [2], [3], however in the case of crystals less perfect than e.g., silicon or diamond it is negligible in comparison to the larger contribution associated with defects. We ignore also the influence of crystal plane bending, because in the case under consideration, as we show in the paper, the investigated epitaxial layers are extensively or almost completely relaxed.

3.2. Substrate's off-cut magnitude and direction

Substrate's off-cut magnitude (α) and direction determination is based on the fact that they affect ω angle at which a symmetrical reflection is found at a given azimuthal angle. Thus, we measured 004 RCs (DA) in GaAs at the following azimuthal angles: 0°, 90°, 180° and 270°. Next, the results (ω angles of the reflection) were fitted by a sine function to calculate the maximal offset (it is the off-cut magnitude) and its azimuthal angle (φ) - it assigns the off-cut direction, see Figure S1.

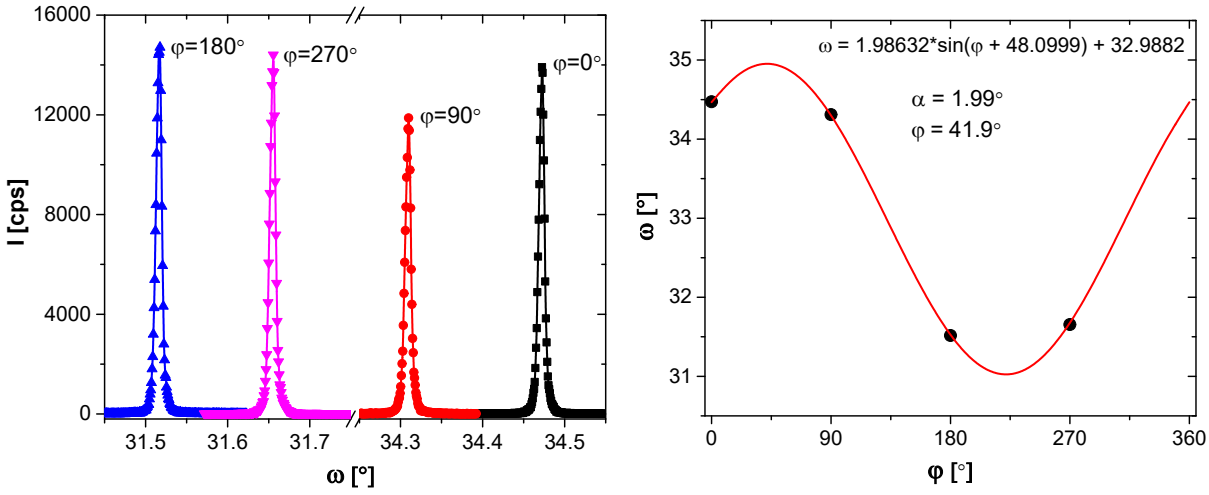

Figure S1. Determination of a substrate's off-cut magnitude and direction based on 004 RCs (DA) measurements at different azimuthal angles – an example for S11 sample.

3.3. Layer's crystallographic plane misorientation (tilt)

Layer's crystallographic plane misorientation was determined analogous to substrate's off-cut: 004 RCs (DA) in CdTe and SnTe were measured at the same four azimuthal angles like for GaAs. Next, the values of maximal offset and its azimuthal angle were calculated.

However, it must be noticed that they are “absolute” values, which are not related to the adjacent layer. Thus, to obtain the correct values of GaAs-CdTe and CdTe-SnTe misorientation (assigned by the same symbol α, like substrate’s off-cut) subsequent calculations were done.

4. Analysis of a strain relaxation in layers

Analysis of a strain relaxation is a complex procedure, involving the following steps:

1) measurement of lattice parameters $a\|$ and $a\perp$,
2) verification of the results of step 1) by checking an order and magnitude of the unit cell distortion,
3) relaxed lattice parameter (a_{relax}) calculation based on the tabularized elastic stiffness constants for the investigated material at the conditions of the experiment,
4) calculation of vertical ($\varepsilon_\perp$) and horizontal ($\varepsilon_\|$) strains,
5) assessment of layers’ thermal strain,
6) calculation of a lattice percentage relaxation.

All of the steps are described below.

4.1. Lattice parameters $a\|$ and $a\perp$

Determining of the unit cell parameters of investigated materials is based on the $2\theta/\omega$-scan curves or reciprocal lattice point maps (RLM) which provide information about the Bragg’s angles (2θ) for each layer. $2\theta/\omega$-scan curves (TTO) are recorded via the analyzer and show the intensity of reflected beam as a function of a detector position (the ω angle, including the scan, also changes with the rate correlated with the change in the angle of the 2θ detector; this speed is twice as low). Reciprocal lattice point maps (RLM) show the distribution of reflected beam intensity around the selected reciprocal lattice point (in fact - this 2D intensity map is measured by multiple $2\theta/\omega$ scans around Bragg angle, with a small varying $\Delta\omega$ detector-sample coupling point).

Figure S2 illustrates exemplary reciprocal lattice point maps of 004 reflections, measured at two orthogonal azimuthal angles (0° vs. 90°) for the samples with different SnTe layer thicknesses: 80, 500 and 1000 nm.

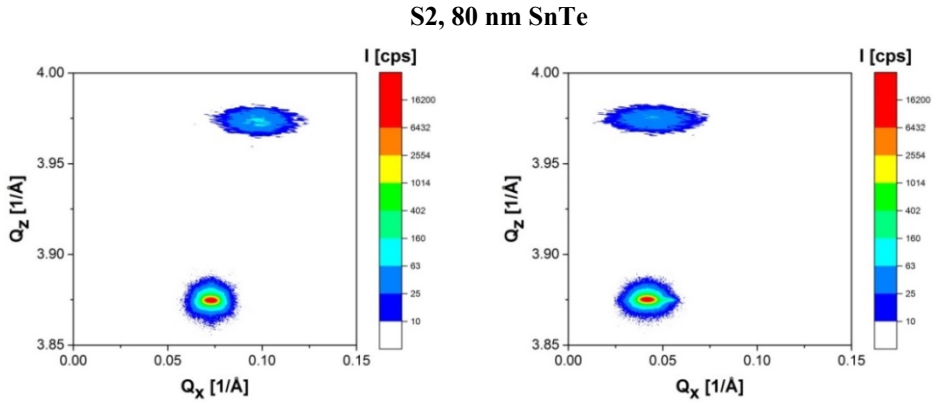

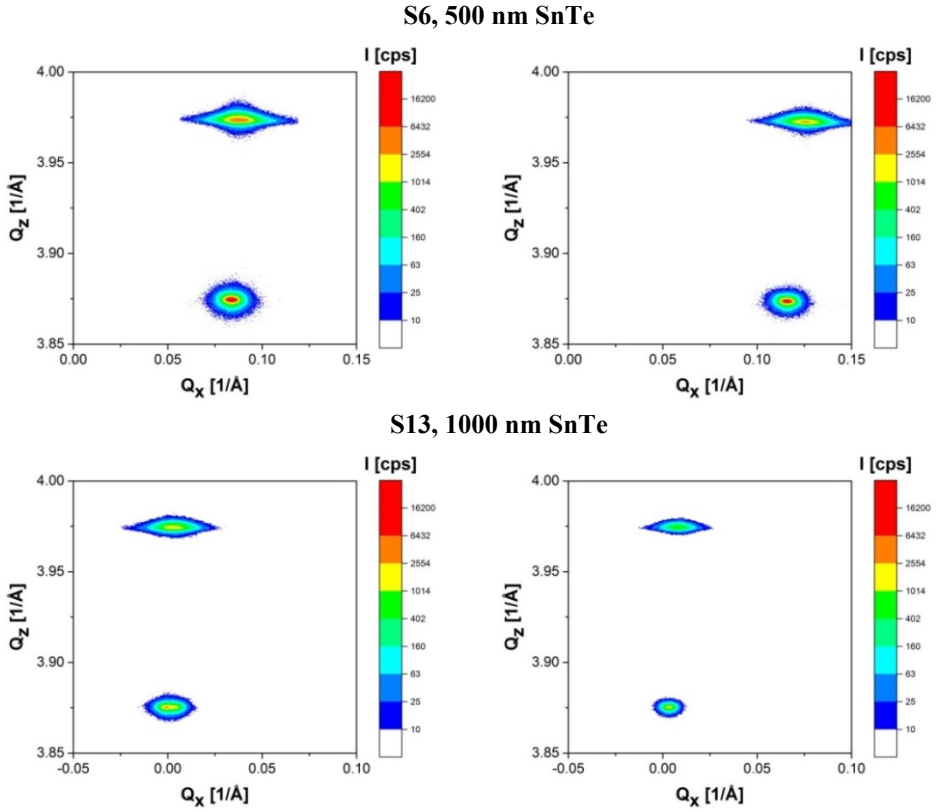

Figure S2. Reciprocal lattice point maps of 004 reflections, measured at two orthogonal azimuthal angles (0° vs. 90°) for the samples with different SnTe layer thicknesses.

The determined Bragg's angles (2θ) values enabled calculation of the lattice parameters accordingly to the assumed crystal symmetry. It should be emphasized that directly from the measurements of the reflections *hkl* we have only easy to determine the interplanar distances d_{hkl}. The use of the appropriate deformation model allows relating the values d_{hkl} determined from the experiment with the parameters of the unit cell. So generally for bulk crystals in the case of GaAs, CdTe and SnTe it is cubic, thus $a_{||}$ value should be equal to $a_{\perp}$. However, in the layered heterostructure interactions between the two crystallographic materials, the bottom one and the one growing on top, can lead to a strong deformation of the latter, thus it is important to check their order to correct the results if applicable.

4.2. Order and magnitude of a unit cell distortion

To check the order of a unit cell distortion from the preliminarily assumed cubic symmetry it is essential to measure 2θ of two set of reflections (symmetrical and asymmetrical) and compare the values of a calculated from them. If the discrepancy is higher than the measurement uncertainty, a significant unit cell distortion occurs. The order of it is at least tetragonal.

Next step was calculation of $a_{||}$ and $a_{\perp}$ using tetragonal model of the unit cell and then checking if the values of $a_{||}$ measured at two orthogonal azimuthal angles are the same. If the discrepancy between them is still higher than the measurement uncertainty the order of the unit cell distortion is higher than tetragonal. In the case of SnTe it was monoclinic (the γ angle between two $a_{||}$ was not equal to 90°).

The calculations of the corrected values of lattice parameters and γ angle for monoclinic structure were based on the mathematical relationship between interplanar distance and lattice parameters (see ref. [4]):

$$\frac{1}{d_{hkl}^2} = \frac{h^2}{a^2 sin^2(\gamma)} + \frac{k^2}{b^2 sin^2(\gamma)} - \frac{2hkcos(\gamma)}{absin^2(\gamma)} + \frac{l^2}{c^2}$$

assuming that $b = a = a_{||}$ and $c = a_{\perp}$.

This equation was simplified for the reflections: $00l_1$ (in our experiment it was 004), $-h\text{-}hl_2$ and $h\text{-}hl_2$ (-2-26 at two perpendicular azimuthal angles 0° and 90°). The families of $00l_1$, $-h\text{-}hl_2$ and $h\text{-}hl_2$ reflections are most convenient for measurement and calculations in the case of such kind monoclinic unit cell distortion as it was revealed in our samples. Assuming $A_{1(2)} = 1/d^2_{\text{-}h\text{-}hl2\ (\text{-}hhl2)}$, where $d_{\text{-}h\text{-}hl2\ (\text{-}hhl2)}$ - interplanar distance for the $-h\text{-}hl_2$ ($-hhl_2$) reflex, we get very simple dependencies: $a_{\perp} = l_1 * d_{00l1}$; $\cos(\gamma) = (A_2\text{-}A_1)/(A_2+A_1\text{-}2*(l_2/(a_{\perp}))^2)$; and $a_{||} = 2h/(\sin(\gamma) * (A_2+A_1\text{-}2*(l_2/(a_{\perp}))^2)^{0.5})$.

The measurement uncertainty for "out of plane" lattice parameter ($a_{\perp}$) amounts to ±0.0002 Å and for the "in plane" ($a_{||}$) ±0.003 Å for both, CdTe buffer and SnTe layers. It is valid for the tetragonal distortion as well as for the monoclinic one.

4.3. Vertical ($\varepsilon_{\perp}$) and horizontal ($\varepsilon_{||}$) strains

The vertical ($\varepsilon_{\perp}$) and horizontal ($\varepsilon_{||}$) strains for CdTe and SnTe are calculated using the following equations from ref. [5]:

$$\varepsilon_{\perp(||)} = \frac{a_{\perp(||)} - a_{relax}}{a_{relax}}$$

where:

$a_{\perp(||)}$ - "out-of-plane" ("in-plane") lattice parameter,

a_{relax} - relaxed lattice parameter.

The relaxed lattice parameter, assuming tetragonal deformation of the layer is calculated according to the formula from ref. [6]:

$$a_{relax} = \frac{a_{\perp} + 2(\frac{C_{12}}{C_{11}})a_{||}}{1 + 2(\frac{C_{12}}{C_{11}})}$$

Where C_{11} and C_{12} are the constants of elastic stiffness at room temperature: for CdTe $C_{11} = 5.351 \times 10^{10}$ N/m^2, $C_{12} = 3.681 \times 10^{10}$ N/m^2 (ref. [7]) and for SnTe $C_{11} = 10.43 \times 10^{10}$ N/m^2, $C_{12} = 0.178 \times 10^{10}$ N/m^2 (ref. [8]).

Calculations of a_{relax} from the constants of elastic stiffness instead of using of the tabularized values of a measured for bulk materials (as an equivalent of a_{relax}) provide more accurate

results of the strains determination due to the fact that the calculated a_{relax} concerns not a bulk material but a relaxed layer in heterostructure, that is to say, it shows how the studied material of the layer relax on a given substrate, according to its elastic properties at a given temperature (which are universal).

4.4. Assessment of layers' thermal strain

To find more complex model of the measured strain in CdTe and SnTe it has been assessed thermal strain of that layers. For the calculations the following equation were applied:

$$\varepsilon_{Therm}^{\ L} = \frac{a_{\parallel}^{L}(T) - a_{relax}^{\ L}}{a_{relax}^{\ L}}$$

where:

$\varepsilon_{Therm}{}^{L}$ - thermal strain (horizontal) of the layer,

$a_{\parallel}{}^{L}(T)$ – calculated "in-plane" lattice parameter of layer in room temperature, on the premise that its growth is held according to its own appropriate thermal expansion coefficient but cooling – according to thermal expansion coefficient of substrate.

4.5. Lattice percentage relaxation

Lattice percentage relaxation R% of the layer 2 relative to the layer 1 is calculated as (see ref. [9]):

$$R\% = \frac{a_{\parallel}^{L1} - a_{\parallel}^{L2}}{a_{\parallel}^{L1} - a_{relax}^{\ L2}} \times 100\%$$

where:

$a_{\parallel(relax)}{}^{L1(L2)}$ - "in-plane" (relaxed) lattice parameter of the appropriate layer.

For calculation of CdTe lattice percentage relaxation we used as $a_{\parallel}{}^{GaAs}$ and $a_{relax}{}^{GaAs}$ the averaged value of not deformed GaAs lattice parameter, from our measurements, equal to 5.6534 Å.

5. Analysis of azimuthal defects distribution

To analyze azimuthal defects distribution we performed a set of measurements of RC FWHM's at different azimuthal angles from 0° to 360° to check if significant fluctuations of FWHM occur.

5.1. Impact of lattice misorientation on RC FWHM measured at various azimuthal angles

The fluctuations of RC FWHM are influenced not only by the azimuthal defects distribution but partially also by the azimuthal dependence of the off-cut angle (α = sin(Phi-Phi$_0$); Phi$_0$ – azimuthal angle for which the diffractometer axis coincides with the line of intersection of the (001) plane with the sample surface). However, its impact is significantly smaller than the changes caused by defect distribution anisotropy. Of course that influence depends on reflection; the largest is for 002, as shows the formula from ref. [9]:

$$FWHM(Phi) = < FWHM_{exp} > * \sqrt{\frac{sin(\theta - \alpha(Phi))}{sin(\theta + \alpha(Phi))}}$$

where:
θ- Bragg angle; $\alpha = sin(Phi\text{-}Phi_0)$.

Table S2 presents magnitudes of FWHM changes with azimuthal angle.

Table S2. Calculated amplitudes of FWHM azimuthal changes.

Layer	reflection	Amplitude of FWHM changes with azimuthal angle (difference of max and min values obtain from simulated function) ["]	
		S11	S10
CdTe	002	97.2	103.8
	004	41.1	46.2
	006	22.2	25.2
SnTe	002	137.2	185.0
	004	60.4	119.9
	006	34.1	42.2

Figure S3 presents exemplary plots for S11 sample with experimental FWHM values as a function of measurement azimuthal angle for 004 and 006 reflections, arranged together with simulated curves, illustrating FWHM changes due to the misorientation of a layer. The plots exemplify an impact of lattice misorientation on RC FWHM. It is clearly visible that this impact is small enough to be ignored in the results' interpretation.

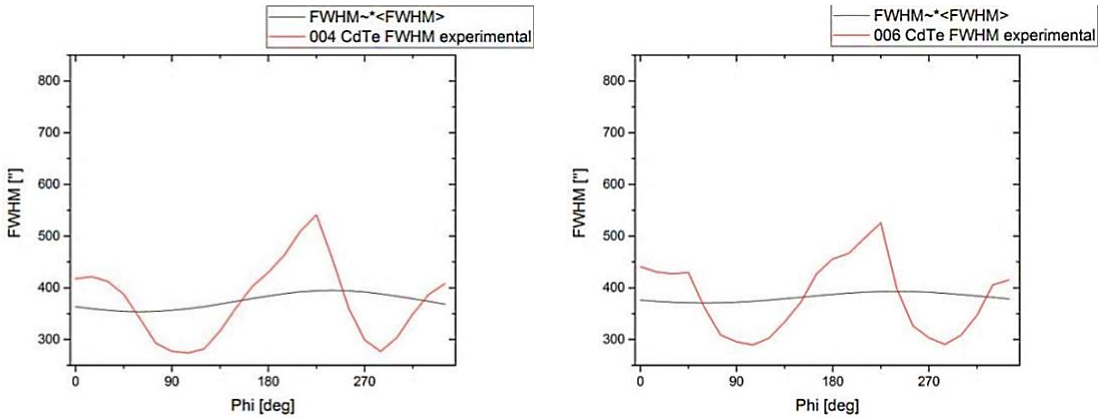

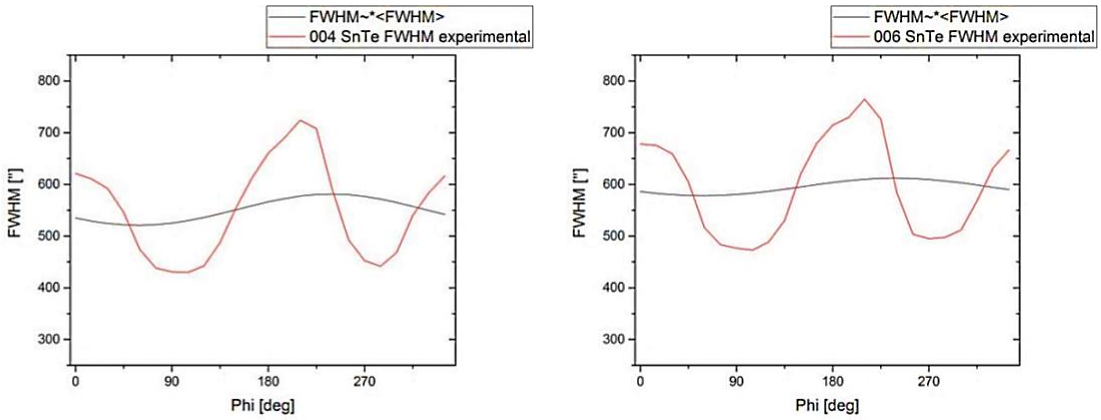

Figure S3. Impact of lattice misorientation on RC FWHM as a function of measurement azimuthal angle for S11 sample; the plot FWHM~*<FWHM> is a simulated curve, illustrating FWHM changes due to the misorientation.

6. Calculation of a dislocations' density

On the base of Ayers plots ($FWHM^2$ as a function of $\tan^2\theta$) [10] to estimate maximal and minimal dislocation density (D) we used the slope (K) of the line passing through the experimental points related to the FWHM's of 002, 004 and 006 reflections, both for CdTe and SnTe layers. For determining FWHM of 002 reflections we had to simulate the RC by two Gaussian functions to separate two maxima situated close to each other. Additionally, we separated in the same manner maxima coming from so-called hybrid reflections [11], which could change FWHM of CdTe reflection. Exemplary Ayers plots, used for calculation of the minimal dislocation density in CdTe in S11 and S10 samples, are shown in the Figure S4.

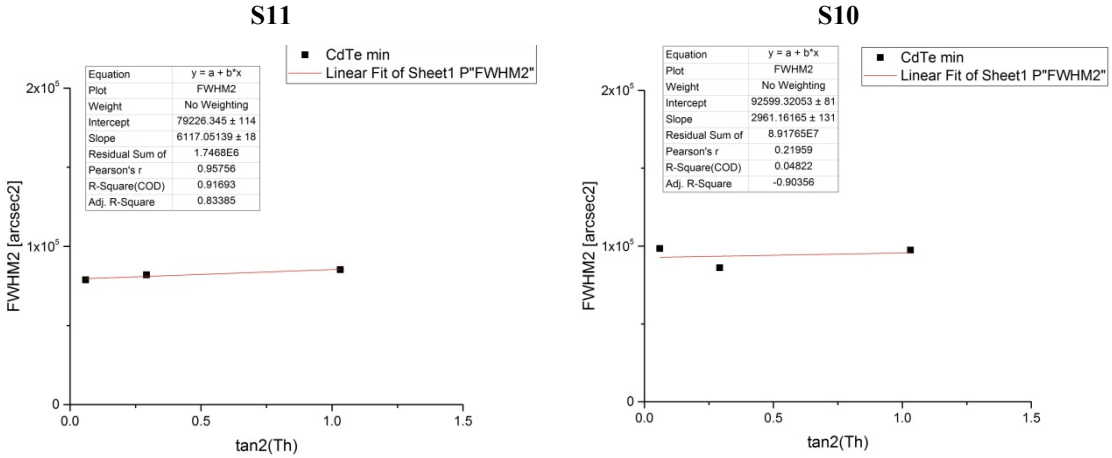

Figure S4. Exemplary Ayers plots for S11 and S10 samples.

The equation applied for calculation of D is following:

$$D = \frac{K}{4.36b^2}$$

where b is a length of the Burger's vector. It is important to remember that K determined in $arcsec^2$ (as in the case of the plots in Figure 4) should be converted to rad^2.

7. Calculation of a micro-strain and a size of grains

We assessed a micro-strain and a size of grains using Williamson-Hall plots – the exemplary plots for the sample S11 are shown in the Figure S5.

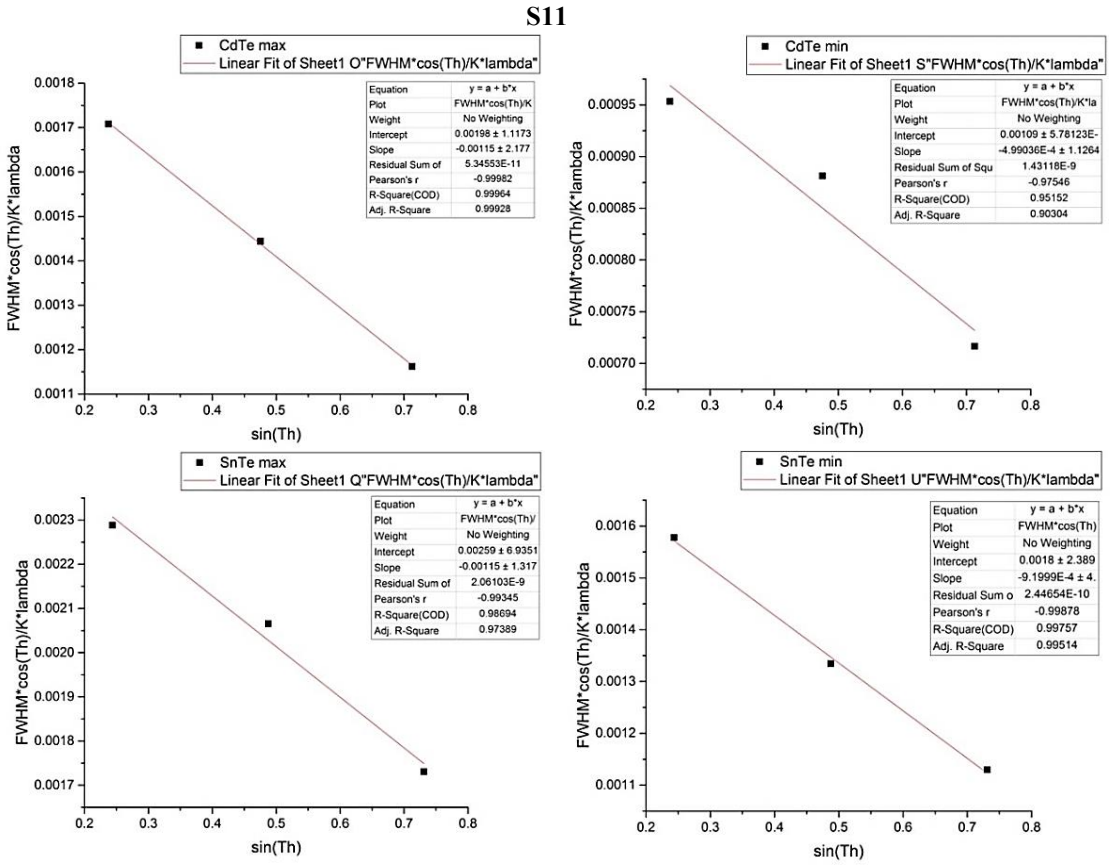

Figure S5. Williamson-Hall plots for the sample S11.

On the grounds of the Williamson-Hall plots we calculated a micro-strain and a size of grains, listed further in Table S3. The values of micro-strain are comparable with the values of vertical strain.

Table S3. micro-strain and a size of grains, calculated on the grounds of Williamson-Hall plots for the samples S10 and S11.

	Micro-strain at defects maximum ($\times 10^4$) CdTe / SnTe	Micro-strain at defects minimum ($\times 10^4$) CdTe / SnTe	Size of grains at defects maximum [nm] CdTe / SnTe	Size of grains at defects minimum [nm] CdTe / SnTe
S11	**-4.0 / -4.0**	**-1.7 / -3.2**	**51 / 39**	**92 / 56**
S10	**-3.0 / -6.0**	**-2.2 / -4.5**	**51 / 32**	**83 / 41**

8. SnTe unit cell distortion vs. surface morphology

Figure S6 shows an impact of crystalline topological insulator unit cell distortion on the samples' surface morphology.

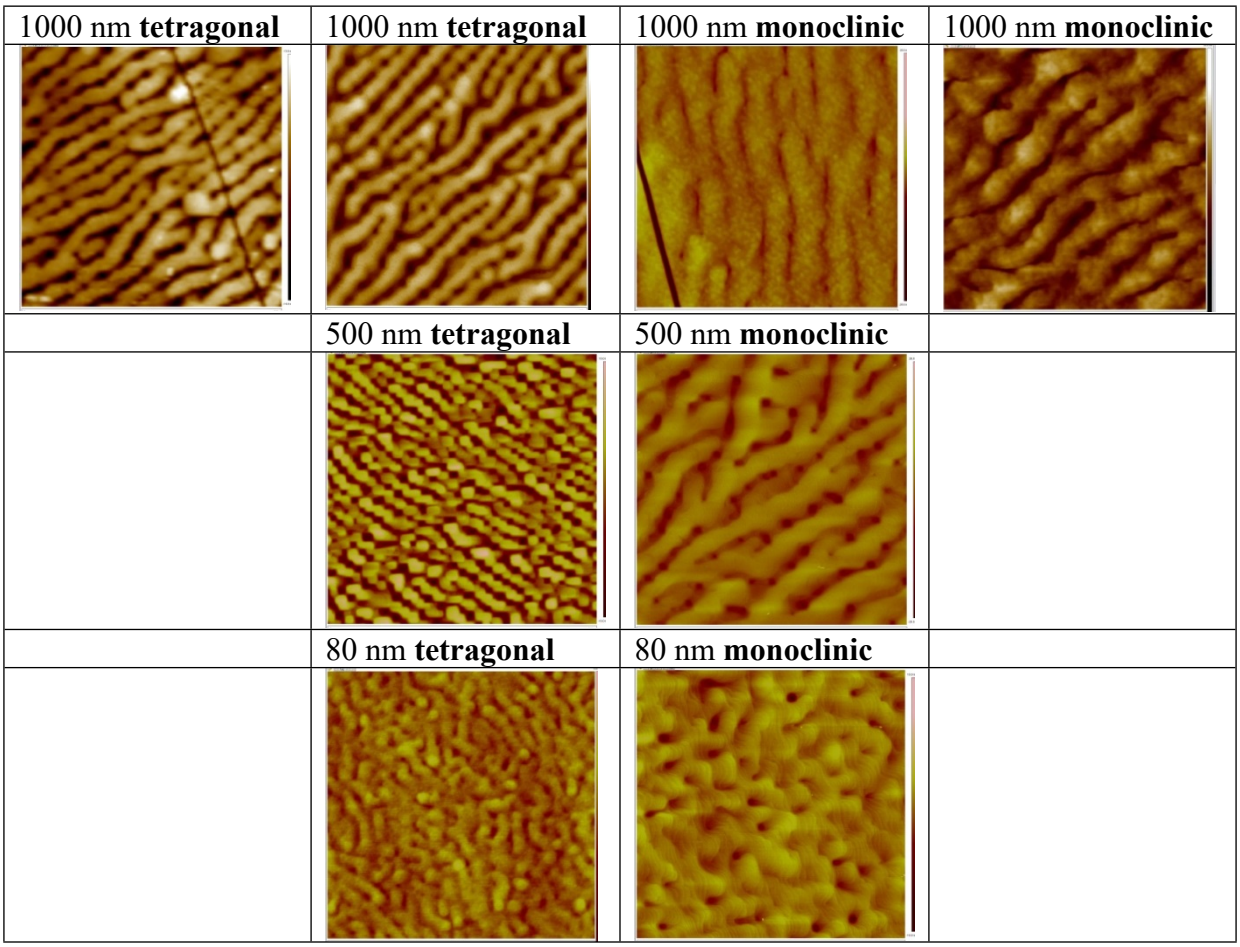

Figure S6. Impact of crystalline topological insulator unit cell distortion on the samples' surface morphology – AFM images of samples with tetragonal vs. monoclinic SnTe. Scale 2μm × 2μm for all images.

As it can be seen, there are noticeable differences in the surface nanostructures width between the samples with tetragonal and monoclinic SnTe unit cell distortion. The nanoripples on the layers with tetragonal SnTe are noticeable narrower than the structures on the layers with monoclinic SnTe.

In the Figure S7 some cracks, generated during cooling the samples after growth, are visible – as thin straight lines on the surface, seen under optical microscope.

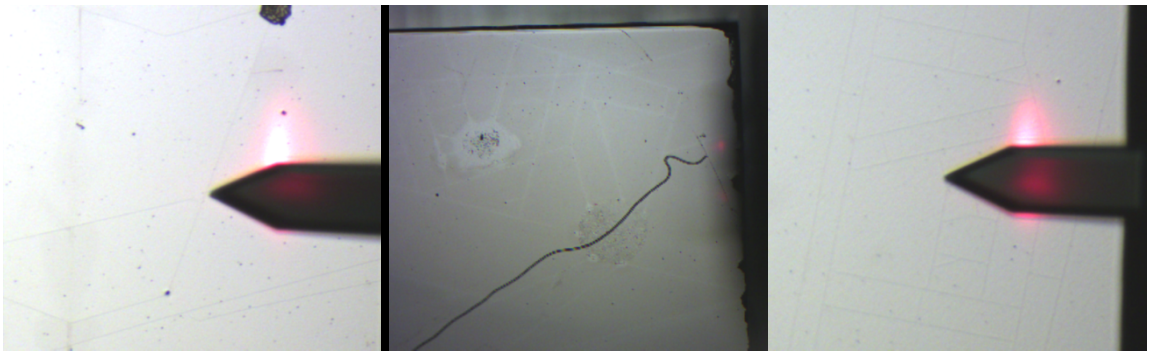

Figure S7. Optical microscope images of samples, disclosing cracks, generated during cooling the samples after growth.

Bibliography

[1] S. Schreyeck, K. Brunner, L. W. Molenkamp, G. Karczewski, M. Schmitt, P. Sessi, M. Vogt, S. Wilfert, A. B. Odobesko and M. Bode, "Breaking crystalline symmetry of epitaxial SnTe films by strain," *Physical Review Materials,* vol. 3, p. 024203 (7 pp.), 2019.

[2] F. Masiello, G. Cembali, A. I. Chumakov, S. H. Connell, C. Ferrero, J. Härtwig, I. Sergeev and P. Van Vaerenbergh, "Rocking curve measurements revisited," *Journal of Applied Crystallography,* vol. 47, no. 4, p. 1304, 2014.

[3] P. F. Fewster, X-Ray Scattering from Semiconductors, London: Imperial College Press, 2000.

[4] M. Martínez-Ripoll, "www.xtal.iqfr.csic.es/Cristalografia/," Dept. de Cristalografia y Biol. Estruc. c/ Serrano 119 E-28006 Madrid (Espania), [Online]. Available: www.xtal.iqfr.csic.es/Cristalografia/parte_04-en.html. [Accessed 3 March 2021].

[5] M. A. Moram and M. E. Vickers, "X-ray diffraction of III-nitrides," *Reports on Progress in Physics,* vol. 72, p. 036502 (40 pp), 2009.

[6] S. Gehrsitz, H. Sigg, N. Herres, K. Bachem, K. Köhler and F. K. Reinhart, "Compositional dependence of the elastic constants and the lattice parameter of AlxGa12xAs," *Physical Review B,* vol. 60, no. 16, pp. 11601-11610, 1999.

[7] D. G. Thomas, "Excitons and Band Splitting Produced by Uniaxial Stress in CdTe," *Journal of Applied Physics,* vol. 32, no. 10, pp. 2298-2304, 1961.

[8] A. J. Miller, G. A. Saunders and Y. K. Yogurtcu, "Pressure dependences of the elastic constants of PbTe, SnTe and Ge0.08Sn0.92Te," *Journal of Physics C: Solid State Physics,* vol. 14, no. 11, p. 1569, 1981.

[9] D. K. Bowen and B. K. Tanner, High Resolution X-Ray Diffractometry and Topography, London; Bristol: PA: Taylor & Francis, 1998.

[10] J. E. Ayers, "The measurement of threading dislocation densities in semiconductor crystals by X-ray diffraction," *Journal of Crystal Growth,* vol. 135, p. 71—77, 1994.

[11] S. L. Morelhão and J. Z. Domagala, "Hybrid reciprocal space for X-ray diffraction in epitaxic layers," *Journal of Applied Crystallography,* vol. 40, p. 546–551, 2007.